

Article

Systematic Evaluation on Speckle Suppression Methods in Examination of Ultrasound Breast Images

Xiangfei Feng ¹, Xiaoyu Guo ¹ and Qinghua Huang ^{1,2,3,*}

¹ School of Electronic and Information Engineering, South China University of Technology, Guangzhou 510641, China; eexffeng@mail.scut.edu.cn (X.F.); guoxiaoyu.zh@ccb.com (X.G.)

² College of Information Engineering, Shenzhen University, Shenzhen 518060, China

³ School of Electronics and Information, and Center for OPTical IMagery Analysis and Learning (OPTIMAL), Northwestern Polytechnical University, Xi'an 710072, China

* Correspondence: qhhuang@scut.edu.cn; Tel: +86-20-8711-3540

Academic Editor: Kohji Masuda

Received: 18 September 2016; Accepted: 8 December 2016; Published: 28 December 2016

Abstract: Breast ultrasound is an important tool used in the medical treatment and diagnosis of breast tumor. However, noise defined as speckles are generated inevitably. Although the existence of speckle may be beneficial to diagnosis if used by a well-trained observer, it often causes disturbance which negatively affects clinical diagnosis, not only by reducing resolution and contrast of ultrasound images, but also by adding difficulties to recognize tumor region accurately. In this paper, we investigate a number of popular de-speckling algorithms, including filters based on frequency domain, filters based on local statistical properties, filters based on minimum mean square error (MMSE), and filters based on Partial Differential Equation (PDE). Two visual measurement evaluation criteria, i.e., Mean to Variance Ratio (VMR) and Laplace Response of Domain (LRD), are chosen for the performance comparison of those filters in the application of ultrasound breast image filtering. Moreover, the filtering effect is further evaluated with respect to the segmentation accuracy of tumor regions. According to the evaluation results, we conclude that Bilateral Filter (BF) achieves the best visual effect. Although Weickert J Diffusion (WJD) and Total Variation (TV) can also obtain good visual effect and segmentation accuracy, they are very time-consuming.

Keywords: breast tumor; speckle suppression; comparison; ultrasound image

1. Introduction

Breast cancer is the second leading cause of cancer death in women after lung cancer. It was estimated that 39,520 women in USA died of breast cancer in 2011 [1]. On current trends, the incidence and death rates of breast cancer are not likely to fall in the near future. Although breast cancer is regarded as one of the most fatal diseases, the earlier tumor is diagnosed, the greater the chance of survival. It is very important to improve the accuracy of breast cancer diagnosis so that patients can have the optimal opportunity of treatment and cure. Currently, ultrasound images are widely used in medical fields, especially the B-mode ultrasound image. Breast ultrasound image (BUS) plays a dominant role in tumor diagnosis and treatment because of its good accuracy, low-expense, non-invasive and applicable nature [2].

However, as a result of the coherent nature of ultrasound imaging, a noise pattern known as a speckle is inevitably generated. The speckle is known to hamper object recognition [3]. The existence of speckle disrupts clinical diagnosis, especially the computer-aided diagnosis (CAD), not only by reducing the image resolution and contrast [4] and hence causing classification errors of the breast tumor, but also by adding difficulties to subsequent image processing, e.g., tumor region segmentation and recognition. Hence, speckle suppression filtering (to achieve smoothness in the homogeneous

region and clearer details in the edge region) is a prerequisite procedure in BUS image processing to promote image quality and tumor segmentation accuracy.

Predecessors have made efforts to analyze the speckles in medical ultrasound images. Speckle pattern is categorized in three classes according to the number of scatterers per resolution cell called scatterer number density (SND). The first one is fully formed speckle (FFS) pattern. The SND of this speckle pattern is larger than 10, and the amplitude of the backscattered signal can be modeled as a Rayleigh (Rayleigh distribution) [5]. Moreover, the Speckle is a form of multiplicative noise triggered by the interference between ultrasound waves [6]. The second one is non-randomly distributed with long-range (NRLR) order [2], which can be modeled by K-distribution or Nakagami distribution. The third one is non-randomly distributed with short-range (NRSR) order [2], and the probability density function (PDF) of the backscattered signal becomes close to Rician distribution. The three classes [7] are associated with a constant Signal Noise Ratio (SNR) of 1.92, below 1.92 [8] and above 1.92, respectively.

Generally, we assume that in some cases, properties of speckle in BUS images are similar to FFS [5] in which the contaminated image model can be expressed as the original one with multiplicative noise. Additionally, image inevitably contains additive Gaussian white noise (GWN) due to the inherent characteristics of communication channel. Therefore, the model of a contaminated image approximately expressed as: $I_g = I_f \cdot n_m + n_a$ [4], where I_f stands for original image, I_g is the contaminated image, n_m is the multiplicative noise and is assumed to obey Generalized Gamma distribution [9], and n_a is the additive GWN. Note that n_m and n_a , which form speckles, can be regarded as degradation function and additive noise, respectively.

Various filtering algorithms have been applied to medical BUS images and achieved good performance for speckle suppression. The existing filtering algorithms can be classified into the following categories: (1) filters based on frequency domain; (2) filters based on the local statistical properties; (3) filters based on the minimum mean square error (MMSE); and (4) filters based on Partial Differential Equation (PDE).

The filtering algorithms based on the information of spectrum can be labeled as filters based on the characteristics of frequency domain. They are applied to de-speckling by inhibiting a region of the spectrum. However, the noise and the location in an image are not relevant to each other. Therefore, we are unable to locate the noise in the frequency domain, which results in the inability to accurately separate the noise from the image. Currently, speckle reduction via filtering in the wavelet domain has aroused concern, e.g., the idea of soft-thresholding de-noising first presented by Donoho [10]. However, two major drawbacks of the thresholding methods should be concerned [11]. Firstly, it is almost impossible to find the optimal solution for all kinds of images. Secondly, it is unadvisable to use the same noise model for the diverse resolutions. Although the wavelet spectrum can present more details than the frequency spectrum, the problem of how to recognize the noise remains unsolved.

For the filtering method based on local statistical properties, adaptive mean filters [12,13] have been proposed. These filters remove speckle noise via local image statistics such as mean and variance, instead of requiring degradation and noise function. In the homogeneous region of the image, filters act like a mean filter, while in the edge region they act like a nearly all-pass filter. However, the performance of de-speckling is constrained by the local statistics that are ineffective in some cases, such as the de-speckling area contains both speckle noise and significant texture. Non-local means (NLM) de-noising [14,15] has been a focus of research in recent years, which is based on the non-local averaging of all pixels in the image. In particular, the weight of each point is proportional to the similarity of its neighborhood with that of the point being filtered. After the non-local means filter was proposed, the concept of non-local was rapidly adopted by other researchers [16,17]. The Bilateral Filter (BF), as a specialization of NLM filter algorithms, has been more widely applied in de-speckling due to its user-friendliness and less time consumption [18].

For the filtering method based on the MMSE, this type of filtering algorithm already proposed for de-speckling [19] includes the process of additive noise suppression and inverse degradation. The goal

is to find the estimated value $I_{\hat{f}}$ of non-contaminated image from I_g by minimizing mean square error between I_g and $I_{\hat{f}}$. In order to obtain $I_{\hat{f}}$, it is necessary to obtain degradation and additive noise function, which is quite difficult because of the characteristic of BUS image. Besides, the MMSE filter is a linear filter and reduces speckle noise with blurring the image [20]. It has been known that linear filters do not perform well in de-speckling since it blurs sharp edges [21], and the sharp edges are very important for segmentation of tumors.

The PDE methods applied to achieve high-quality image de-noising have attracted extensive attention [7,22]. The diffusion filtering category includes isotropic model such as Perona–Malik diffusion (PMD) filter [23], anisotropic model such as Weickert J Diffusion (WJD) filter [24], and another diffusion model such as Total Variation (TV) filter which was first proposed by Rudin et al. [25]. In PMD model, the value of diffusion coefficient is only relevant to the magnitude gradient of image. However, according to WJD and TV models, both the value and direction of diffusion are taken into account. Therefore, the PMD model is the simplest one among these three algorithms, but is more sensitive to noise.

In the past decades, a large amount of algorithms have been proposed to contribute to medical ultrasound image filtering, and some works have been done to compare their performances. Loizou et al. [26] has compared 10 de-speckle filters in ultrasound images of the carotid artery bifurcation based on texture analysis, image quality evaluation metrics, and visual evaluation. Finn et al. [27] described fifteen speckle filters for the application of echocardiography, and it also discussed the computational performance of the filters. Manth [28] evaluated the performance of de-speckle filters by using a dataset of 64 B-Mode liver ultrasound images based on three kinds of measurements. Zhang et al. [29] made a comparison of eleven de-speckle filters for the BUS images and simulated images based on several comparing methods, such as blind image quality metric (NIQE). However, it did not discuss the computational performance of the filters and the filtering effect for the subsequent processing, such as segmentation. Kaur et al. [30] made a comparison of eleven spatial de-speckling filters for Ultrasound based on some performance metrics, such as mean square error. However, there are a lot of de-speckling filters which are not spatial filters, such as Wavelet Transform Filter (WTF).

Motivated by the application of ultrasound breast images, we systematically evaluate eight de-speckling filters according to the categories of filters discussed above. The evaluation consists of the performance of visual measurement, the filtering effect on tumor region segmentation accuracy and computational performance. In relation to the BUS images, the degree of approximation of the estimated image cannot be measured due to the inaccessible original image. Hence, reasonable parameters should be set to compare and analyze the performance among different types of filtering algorithms. In most cases, not only us, but also the doctors pay close attention to the visual measurement. This includes the degree of smoothness in the homogeneous region and the clarity of detailed features in the edge region. In this paper, Mean to Variance Ratio (VMR) [31] which is also named as equivalent number of looks and Laplace Response of Domain (LRD) [32] are chosen to evaluate the key performance, i.e., the degree of smoothness in the homogeneous region and clarity of edge detailed features in the edge region, respectively. Moreover, we show the filtering effect on tumor region segmentation accuracy. Referring to experimental results, a general conclusion discusses the cause of different performances between different filters, parameter settings and improvement of some certain filters.

2. Filtering Methods

For speckle suppression of medical ultrasound breast image, we can broadly categorize the filtering algorithms and compare the performances among different filtering algorithms to find the most preferred one. Because of numerous applications and versatility of de-speckling filters, this paper is unable to discuss all proposed filters. In this paper, we discuss eight typical filtering algorithms

according to the filter categories discussed above: WTF, Gaussian–Laplace Filter (GLF), Lee Filter (LF), BF, Wiener Filter (WF), PMD, WJD, and TV.

2.1. Frequency Domain–Based Filter

Wavelet Transform Filter

WTF is based on wavelet theory and performs in the wavelet domain. The original signal will be transformed to the wavelet domain by Wavelet Transform. For the reason that the sparsity of wavelet coefficient, i.e., a few large coefficients contains most of information of the signal, the filtering processing can perform according to a threshold. After the idea of soft-thresholding de-noising first presented by Donoho [10], many researchers [33–35] tend to apply the WTF filter to de-speckling of the medical ultrasound image. Generally, WTF can be expressed as follows

$$I_f^\wedge(t) = \frac{1}{C_\varphi} \iint W_\varphi(s, \tau) \frac{\varphi_{s,\tau}(t)}{s^2} d\tau ds \tag{1}$$

where $C_\varphi = \int (|\psi(u)|^2/|u|)du$, $\psi(u)$ is the Fourier Transform of $\varphi(t)$, and $W_\varphi(s, \tau)$ with modified wavelet coefficients is the Wavelet Transform of speckle image $I_g(t)$, s is a positive value and defines the scale of WTF and τ is a real number and defines the displacement of WTF.

In this method, the decomposition of a signal in wavelet domain and its wavelet coefficients can be obtained. For the de-noising processing, wavelet coefficients lower than certain threshold values are modified to zero. Finally, the reconstruction of the estimated image can be derived by inverse wavelet transform with processed coefficients.

2.2. Local Statistical-Based Filter

2.2.1. Gaussian Laplace Filter

GLF is a kind of filter which both considers de-noising and edge protecting of an image. As most edge detail locate in the high frequency region, high pass Laplace filter can be regarded as an effective and simple example in images to preserve edge detail [36]. Nevertheless, filtering performance is highly limited because of high sensitivity to noise and natural contradiction between de-noising and retaining details of edge. To this end, it is essential for Gaussian smoothing to be used in cooperation with a Laplace filter for BUS images [37]. GLF [32] can be shown as

$$I_f^\wedge(x, y) = I_g(x, y) \times h(x, y) + \nabla^2(I_g(x, y) \times h(x, y)) \tag{2}$$

where $\nabla^2 = \frac{\partial^2}{\partial x^2} + \frac{\partial^2}{\partial y^2}$, $h(x, y) = \frac{1}{\sqrt{2\pi}\sigma} \exp(-\frac{x^2+y^2}{2\sigma^2})$ is a Gaussian function, and σ is the standard deviation. As illustrated above, GLF is obviously composed of two parts. One is for de-noising, and the other is for edge enhancement.

2.2.2. Lee Filter

The LF is based on local statistics [12] proposed by Lee [38], and dealing with the multiplicative noise signal. Many researchers have used the LF for de-speckling in Synthetic Aperture Radar (SAR) images [39,40]. Insana [41] indicates that the LF can also perform well for the medical ultrasound breast image. Based on the properties of LF, images can be converted into a linear expression regardless of whether it contains additive or multiplicative noise.

Therefore, this is appropriate for the BUS image in which multiplicative noise and additive noise coexist. The LF function for this compounded noise can be expressed as

$$I_f^\wedge = I_f + k(I_g - \bar{n}_m \cdot I_f - \bar{n}_a) \tag{3}$$

Notation n_m is the multiplicative noise and n_a is the additive noise. I_f , I_g , $\overline{n_m}$ and $\overline{n_a}$ stand for the mean of I_f , I_g , n_m and n_a , respectively. In addition,

$$k = \frac{\overline{n_m} \cdot Q}{I_f^2 \cdot \sigma_2^2 + \overline{n_m}^2 \cdot Q + \sigma_1^2} \text{ and } Q = \frac{\text{var}(I_g) + I_g^2}{\sigma_2^2 + \overline{n_m}^2} - I_f - \sigma_1^2 \tag{4}$$

where σ_1^2 is the variance of n_a , σ_2^2 is the variance of n_m , and $\text{var}(I_g)$ is the variance of I_g .

As the speckled medical ultrasound image can be described as $I_g = I_f \cdot n_m + n_a$, the Lee filtering algorithm seems to be effective. However, in fact, when it is used in BUS images, failure arise in accurately estimate the mean and variance of n_m , which may affect the performance of the suppression of multiplicative noise.

2.2.3. Bilateral Filter

BF is a specialization of non-local mean filter. It extends the concept of Gaussian smoothing by weighting the filter coefficients with a corresponding penalty for difference of pixel intensity between the pixel to be filtered and its neighboring pixels. The output of the BF is a weighted average of its neighboring pixels. The BF was first introduced by Aurich et al. [42] by using the name of “non-linear Gaussian filter”, and then rediscovered by Tomasi et al. [43] who gave it the current name. Due to the simplicity and good performance in edge preservation, many researchers highly praised this method and applied it for de-speckling medical ultrasound images [18]. BF is defined as

$$I_f^\wedge(x, y) = \frac{\sum_{kl} I_g(k, l) W_d(x, y, k, l) W_r(x, y, k, l)}{\sum_{kl} W_d(x, y, k, l) W_r(x, y, k, l)} \tag{5}$$

and,

$$W_d(x, y, k, l) = \exp\left(-\frac{(x - k)^2 + (y - l)^2}{\sigma_d^2}\right), W_r(x, y, k, l) = \exp\left(-\frac{[I_g(x, y) - I_g(k, l)]^2}{\sigma_r^2}\right) \tag{6}$$

where σ_d and σ_r are the parameters affecting low-pass filter and the degradation function separately.

It can be indicated that the smoothing degree in the homogeneous region of image depends on σ_d . The higher σ_d is, the smaller cut-off frequency of the Gaussian low-pass filter is. The gray value of homogeneous region is more close to the Direct Current (DC) component.

Assuming that $I_{f(x,y)} = C$, (x, y) belongs to the homogeneous region, and the contaminated image is $I_g = I_f \cdot n_m + n_a$, where n_a is GWN, we have

$$F(0) \xrightarrow{FT} I_f^\wedge(x, y) = \text{mean}(I_g(x, y)) = \text{mean}(I_f(x, y) + n_a) \tag{7}$$

and

$$I_f^\wedge(x, y) = \text{mean}(I_f(x, y)) = C, \text{ and } \text{var}(I_f^\wedge(x, y)) = 0 \tag{8}$$

Where $\text{mean}(\cdot)$ operator means to calculate the mean value of an image, and $\text{var}(\cdot)$ operator means to calculate the variance of an image. As shown above, in the homogeneous region of an image, the de-noising result is equal to the expectation of the neighbor, such as de-noising by a low-pass filter with the cut-off frequency zero. However, we cannot just increase σ_d because greater σ_d leads to more loss of edge information. Thus, in order to preserve the smoothness of homogeneous region and sharpness of the edge region, both σ_r and σ_d need to be adjusted simultaneously. The relationship between σ_d and σ_r can be calculated by the fixed LRD [32] as the following

$$\nabla^2[I_f^\wedge(x, y)] = C \tag{9}$$

Then

$$C = \nabla^2 [I_f(x, y)] = \nabla^2 \left[\frac{\sum_{kl} I_g(k, l) W_d(x, y, k, l) W_r(x, y, k, l)}{\sum_{kl} W_d(x, y, k, l) W_r(x, y, k, l)} \right] \tag{10}$$

If $I_g(k, l)$ and LRD are kept constant, we can then obtain:

$$\sigma_d^2 \propto 1/\sigma_r^2 \tag{11}$$

The Equation (11) means that when increasing σ_d , in order to keep LRD unchanged, σ_r should be decreased simultaneously.

2.3. MMSE-Based Filter

Wiener Filter

As one of the MMSE methods, Wiener filtering algorithm proposed by Wiener achieves optimal results on average based on the statistic minimization criterion [44], and it has been widely applied. The main idea of WF is to minimize mean square error between the filtered image and its original image. It can filter the noise of image and protect details of image, simultaneously. Modified filter algorithms [45] have represented their usefulness in de-speckling of medical ultrasound image. WF is expressed as follows

$$\hat{F}(u, v) = \left[\frac{H^*(u, v)}{|H(u, v)|^2 + S_n(u, v)/S_g(u, v)} \right] G(u, v) \tag{12}$$

or,

$$\hat{F}(u, v) = \left[\frac{1}{H(u, v)} \frac{|H(u, v)|^2}{|H(u, v)|^2 + S_n(u, v)/S_g(u, v)} \right] G(u, v) \tag{13}$$

where $H(u, v)$ is the degradation function, $H^*(u, v)$ is conjugate with $H(u, v)$, $G(u, v)$ is the frequency representation of $I_g(x, y)$ and $\hat{F}(u, v)$ is the estimated value of $I_g(x, y)$ in frequency space, and $S_g(u, v)$ and $S_n(u, v)$ denote the frequency spectrum of contaminated image and noise, respectively. However, $S_g(u, v)$ is hard to obtain in real application such that $S_n(u, v)/S_g(u, v)$ is often set to be a constant K_{SNR} to find the best visual effect.

Equation (13) is known as the famous WF formula. However, the essential condition of using WF is to find the degradation function and both the power density spectrum of contaminated image and noise in a linear and position-invariant system, which is hard to realize.

2.4. PDE-Based Filter

2.4.1. Perona–Malik Diffusion Filter

PMD filter is a kind of filter based on the anisotropic diffusion theory, which can both de-noise and maintain boundaries. Perona and Malik [23] studied the isotropic diffusion filter or equivalent Gaussian smoothing, and pointed out that Gaussian blurring does not “respect” natural object boundary. Therefore, they introduced a diffusion coefficient which can automatically adjust the diffusivity according to varied image content. This simple diffusion model has been applied to de-speckling of medical ultrasound images [22].

The PMD [23] filter is described as

$$\begin{cases} \frac{\partial I_g}{\partial t} = \text{div}(c(x, y, t) \cdot \nabla I_g) \\ I_g(t = 0) = I_0 \end{cases} \tag{14}$$

In Equation (14), $c(x, y, t)$ is diffusion coefficient which is chosen locally as a function for the magnitude of the gradient of the image, e.g., $c(x, y, t) = g(\|\nabla I_g(x, y, t)\|)$, ∇ is the gradient operator.

The function $g(\cdot)$ is a non-negative monotone decreasing function with $g(0) = 1$. Two functions were proposed to model the diffusion coefficient

$$g(\|\nabla I_g\|) = e^{-(\|\nabla I_g\|/K)^2} \tag{15}$$

and,

$$g(\|\nabla I_g\|) = \frac{1}{1 + (\|\nabla I_g\|/K)^2} \tag{16}$$

where K is a constant controlling the sensitivity of the diffusion coefficient to image gradient and it is usually chosen depending on optimized experiments of visual measurement.

2.4.2. Weickert J Diffusion Filter

WJD filter is also a kind of filter based on anisotropic diffusion theory. During the diffusion process, it chooses a large diffusion coefficient at the direction vertical to the edge direction while a small diffusion coefficient at the direction parallel to the edge direction to protect the local details of image. WJD filter is a modified filter from PMD, aiming to realize the anisotropy diffusion in the discontinuous edge of image. Weickert et al. [24] replaced the diffusion coefficient $c(x, y, t)$ in PMD with a second order structure tensor D . This change greatly improves the diffusion model in de-noising effect, and it has been used for de-speckling medical ultrasound image [7]

$$\frac{\partial I_g}{\partial t} = \text{div}(D\nabla I_g) \tag{17}$$

where $D \in R^{2 \times 2}$ is a symmetry positive semi-definite diffusion tensor. The diffusion tensor D can be represented by its eigenvalues and eigenvectors

$$D = (w_1 \ w_2) \begin{pmatrix} \lambda_1 & 0 \\ 0 & \lambda_2 \end{pmatrix} (w_1 \ w_2)^T \tag{18}$$

where λ_1 and λ_2 are the eigenvalues, and w_1 and w_2 are the eigenvectors.

D can be described as a multi-scale structure matrix [46] which takes the following form

$$J_\rho(\nabla I_\sigma) = \begin{bmatrix} J_{11} & J_{12} \\ J_{21} & J_{22} \end{bmatrix} = K_\rho \times (\nabla I_\sigma \cdot \nabla I_\sigma^T) \tag{19}$$

where I_σ is denoted as the homogeneous region of the pre-smoothed image of contaminated image I_g , and the pre-smoothing is to prevent mistaking speckles for edges by a Gaussian function with standard deviation σ . K_ρ is a Gaussian kernel with standard deviation ρ . The matrix $\nabla I_\sigma \cdot \nabla I_\sigma^T$ is further smoothed by the Gaussian kernel K_ρ . Subsequently, eigenvalue decomposition is performed on $J_\rho(\nabla I_\sigma)$ to obtain w_1 and w_2 .

$$J_\rho(\nabla I_\sigma) = (w_1 \ w_2) \begin{pmatrix} \lambda_1 & 0 \\ 0 & \lambda_2 \end{pmatrix} (w_1 \ w_2)^T \tag{20}$$

To enhance the image local structures, Weickert [24] redesigned the eigenvalues λ_1 and λ_2 in two models as below

Coherence model 1:

$$\begin{aligned} \lambda_1 &= \alpha \\ \lambda_2 &= \begin{cases} \alpha & \text{if } \lambda_1 = \lambda_2 \\ \alpha + (1 - \alpha) \exp\left(\frac{-C}{(\lambda_1 - \lambda_2)^{2m}}\right) & \text{else} \end{cases} \end{aligned} \tag{21}$$

Coherence model 2:

$$\begin{aligned} \lambda_1 &= 1 - \exp\left(\frac{-C}{(|\nabla I_\sigma|/K)^m}\right) \\ \lambda_2 &= 1 \end{aligned} \tag{22}$$

where α is often a small positive number, m is a real number, C is a constant greater than zero, and K is a constant controlling the sensitivity to image gradient. Via λ_1 the vector along the edge direction is obtained, and via λ_2 the vector vertical to the edge direction is obtained. Model 2 is the function of the value of gradient, thus in order to consider the impact of the value and direction of gradient on the diffusion more clear, we prefer to choose Model 2 as the algorithm evaluated in the experiments.

2.4.3. Total Variation Filter

TV Filter is also a filter method according to variational method, which minimizes a specific energy function to perform de-noising of an image. It performs as a diffusion processing. The diffusion direction of TV filter vertical to the gradient direction of image, and the direction parallel to gradient direction of image have a diffusion coefficient zero, thus it can both de-noise and protect the details of edges. The TV Filter was introduced by Rudin et al. [25]. Nowadays, TV used in de-speckling for medical ultrasound images has gained an excellent effect [47]. It has attracted the attention of many researchers. The total variation of an image is the integral of the absolute gradient of an image. It has been proposed that an image with excessive details and noises can have high total variation. Minimizing the total variation of an image can remove the noise whilst preserving important edges. As a result, the process is equivalent to the following total variation minimization problem:

$$\text{minimize} \int_{\Omega} \sqrt{I_x^2 + I_y^2} dx dy \tag{23}$$

$$\text{with} \int_{\Omega} I_f dx dy = \int_{\Omega} I_g dx dy \tag{24}$$

$$\text{and} \int_{\Omega} \frac{1}{2} (I_f - I_g)^2 dx dy = \sigma^2 \tag{25}$$

where I_f is the desired image, and Ω denotes as the region of image. I_x and I_y represent the two vectors of the 2-D image I_f about the gradient, and σ is the standard deviation of GWN.

The first constrain in Equation (24) ensures that the volume covered by the surface of the image remains unchanged during the minimization process. The second constrain in Equation (25) can be derived by the estimated variance of noise as important priori information.

With the Lagrange multiplier β , the minimization problem can be interpreted as

$$\text{minimize} \int_{\Omega} \sqrt{I_x^2 + I_y^2} + \beta (I_f - I_g)^2 dx dy \tag{26}$$

The corresponding Euler–Lagrange equation is

$$0 = \frac{\partial}{\partial x} \left(\frac{I_x}{\sqrt{I_x^2 + I_y^2}} \right) + \frac{\partial}{\partial y} \left(\frac{I_y}{\sqrt{I_x^2 + I_y^2}} \right) - \beta (I_f - I_g) \tag{27}$$

with

$$\frac{\partial I_f}{\partial n} = 0 \text{ on } \partial\Omega \tag{28}$$

where $\partial\Omega$ is the boundary of Ω . Using the gradient projection method, we get

$$\frac{\partial I_f}{\partial t} = \frac{\partial}{\partial x} \left(\frac{I_x}{\sqrt{I_x^2 + I_y^2}} \right) + \frac{\partial}{\partial y} \left(\frac{I_y}{\sqrt{I_x^2 + I_y^2}} \right) - \beta(I_f - I_g) \tag{29}$$

This is a forward time evolution process, i.e., $t > 0$. When the process evolves to a steady state Equation (28), the recovered image is obtained. The TV Filter is efficient at simultaneously preserving edge and smoothing noise. It keeps a strong diffusion in the homogeneous region where the image gradient is relatively small.

2.4.4. Analysis of PDE Filtering Methods

As the PDE filtering methods have achieved good performance in de-speckling for ultrasound images [7], it is necessary to discuss their details here. By observing the three algorithms of the PDE methods, a diffusion model can be divided into isotropic diffusion and anisotropic diffusion, and simply expressed as: $I_f(t) = I_g(t) + \varphi$, where φ is the diffusion function, $I_g(t)$ is the contaminated image, and $I_f(t)$ is the result of diffusion. In isotropic diffusion, φ is the function of $|\nabla I_g(t)|$. While in anisotropic diffusion, φ is the function of $\nabla I_g(t)$. Then the characteristics of PDE can be drawn as follows.

- (1) Either isotropic or anisotropic diffusion can improve the clarity of the edge detail. It can make a blurred region be sharper after diffusion.
- (2) In the case of ignoring the influence of additive noise, the diffusion process can be expressed as the process of convergence from blurred edges to ideal ones.

Additive noise in medical ultrasound images, however, has brought greatly negative effects to the diffusion process. For instance, in the WJD model, additive noise can be mistaken as the edge part. Moreover, in the TV model, additive noise leads to serious influence on the total variation minimization process. That is to say, the diffusion process tends to be regarded as an inverse degradation process, but little related to the removal of additive noise. Therefore, we usually conduct image de-noising for additive noise before diffusion in medical ultrasound images. From the histogram of image in smoothing area, we can easily find that additive noise is similar to a GWN. As a result, many filters based on the diffusion method choose the Gaussian low-pass filter to restrain noise.

Furthermore, for the process of inverse degradation, we can use the property of the diffusion equation to make the blurred edge converge to the ideal edge. In practical applications, the diffusion cannot be completed at once, but as an iterative process:

$$I_f(t) = I_{g_n}(t) = I_{g_0}(t) + \varphi(\nabla I_{g_0}(t)) + \varphi(\nabla I_{g_1}(t)) \dots \varphi(\nabla I_{g_{n-1}}(t)) \tag{30}$$

where $I_{g_n}(t)$ stands for the result after n times iterative processing.

When $n \rightarrow \infty$, we obtain

$$I_f(t) \rightarrow \delta(t), \text{ and LRD} \rightarrow \nabla^2[\delta(t)] \tag{31}$$

and,

$$I_f(t) = I_{g_n}(t) - I_{g_0}(t) = \sum_i^n \varphi_i \tag{32}$$

where φ_i denotes the function $\varphi(\nabla I_{g_i}(t))$. Therefore, the value of the LRD depends on the values φ_i and n .

For the same diffusion results, we can increase φ_i to reduce the iterative time. However, in fact, the greater φ_i enhances the negative impact of noise. Assuming that there is a pulse as noise, if $\varphi_i' > \varphi_i$, then

$$I_{g_n}(t) - I_{g_0}(t) = \sum_i^n \varphi_i' > \sum_i^n \varphi_i \tag{33}$$

Obviously, we need to set φ_i rationally to reach the balance between iterative time and noise-sensitiveness.

3. Evaluation Criteria Analysis for De-Speckling Performance

In this section, evaluation criteria are applied for quantitative evaluation of de-speckling and image segmentation accuracy. Subsequently, we show the mathematical expression of the criterion, experimental description as well as the parameter setting of filters.

3.1. Significance of the Visual Measurement

The non-availability of the original image of BUS image leads to the difficulty in channel estimation. That is to say, the degradation function cannot be accurately estimated. Therefore, the restoration for medical ultrasound image seems to be very difficult. However, in practical applications, such as medical diagnosis, we tend not to require image restoration. On the contrary, we are concerned more about the visual measurement, which consists primarily of the smoothness of the image in the homogeneous region and the clarity of edge characteristic of edge region. For the same instance, mean and standard deviation were applied to evaluate filtering algorithms [3], and Laplace response was used to evaluate the sharpness degree of filtered images [32]. In that way, a contaminated medical ultrasound image $I_g = I_f \cdot n_m + n_a$ [4] can be seen as the homogeneous area which is polluted by additive noise, and the edge of the area becomes vague caused by the degraded function. Therefore, we regard the de-noising and inverse degradation process as: (1) improvement of the smoothness in the homogeneous region; and (2) sharpening the details of the edge region.

3.2. De-Noising Process to Improve the Smoothness

In order to measure the extent of the de-noising, some indices have been proposed, such as VMR [31], Speckle Suppression Index (SSI) [48], Speckle Suppression and Mean Preservation Index (SMPI) [49], and Mean Preservation Speckle Suppression Index (MPSSI) [50]. The SSI is a filtering evaluation index derived from the VMR, which is similar to the normalization processing of VMR. The SMPI and MPSSI are two indices modified from the VMR and SSI, which focus on solving the problem that the filter overestimates the mean value [49] in real applications. However, we choose the VMR as a general measure of the parameter to perform evaluation without considering more complicated situations. The VMR is defined as

$$\text{VMR} = \frac{1}{\text{MR}} \tag{34}$$

where $\text{MR} = \left(\frac{\sigma}{\mu}\right)^2$, μ and σ are the mean and standard deviation of an image, respectively.

Obviously, for a homogeneous region where the mean value is certain, larger VMR indicates a higher degree of smoothing because better filter will get a smaller variance in the homogeneous region. In practical applications, the normalized parameter can be expressed as

$$\begin{aligned} \text{MR} &= \left(\frac{\hat{\sigma}}{\hat{\mu}}\right)^2 / \left(\frac{\sigma}{\mu}\right)^2 \\ \text{VMR} &= \frac{1}{\text{MR}} \end{aligned} \tag{35}$$

where $\hat{\mu}$ and $\hat{\sigma}$ are the mean and standard deviation of the filtered image, respectively; and μ and σ are those of original image. Usually, in order to avoid the edge information eroding accuracy of VMR, we only calculate the VMR in the homogeneous area of image.

3.3. Inverse Degradation Process to Improve the Clarity of the Edge

In order to measure the degree of inverse degradation, we choose the LRD as a measure of filtering effect. The LRD is defined as

$$\text{LRD} = \iint_{x,y} \left| \nabla^2 [I_f^\wedge(x,y)] \right| dx dy \quad (36)$$

where ∇^2 is the Laplace Operator, and (x,y) belongs to edge region.

Clearly, the Laplace response reflects the amount of information in the high-frequency spectrum region. Sharper edges and more details result in stronger Laplace responses. In practical applications, normalized LRD can be expressed as

$$\text{LRD} = \frac{\iint_{x,y} \left| \nabla^2 [I_f^\wedge(x,y)] \right| dx dy}{\iint_{x,y} \left| \nabla^2 [I_f(x,y)] \right| dx dy} \quad (37)$$

where (x,y) belongs to the edge region of original image. Typically, under the influence of noise, the LRD of original image is often greater than that of filtered image.

3.4. Tumor Region Segmentation Accuracy

Image filtering is an important step in image preprocessing. It serves subsequence image analysis such as the segmentation. Speckle suppression filter is expected to debase the influence of speckle noise and improve the segmentation accuracy of region of interest (ROI). To this end, we apply Fuzzy C Mean (FCM) algorithm [51] in segmentation of tumor regions of BUS images which are filtered by the algorithms investigated in this study and evaluate their performances by comparing the segmentation accuracies.

The performance of segmenting tumor region is evaluated by using a metric called averaged radical error (ARE). As reported in [52–55], it is defined as

$$\text{ARE}(n) = \frac{1}{n} \sum_{i=0}^{n-1} \frac{|Cs(i) - Cr(i)|}{|Cr(i) - Co|} \times 100\% \quad (38)$$

In Figure 1, the solid line denotes the “true” boundary of an object and the dashed line denotes the boundary produced by the image segmentation. A number of radius vectors which are evenly spread with Co as their center are emitted from the center of the object. The ratios of the distance from $Cr(i)$ to $Cs(i)$ to that from $Cs(i)$ to $Co(i)$, $i = 1 \dots n$, is summed up and then averaged to obtain the ARE. The “true” delineation is obtained by manual tracing carried out by 3 radiologists. An example of estimated delineation is the boundary of the tumor region segmentation result, as illustrated in Figure 2. The red curve represents the “true” delineation, and the pink curve is the boundary of the segmentation result.

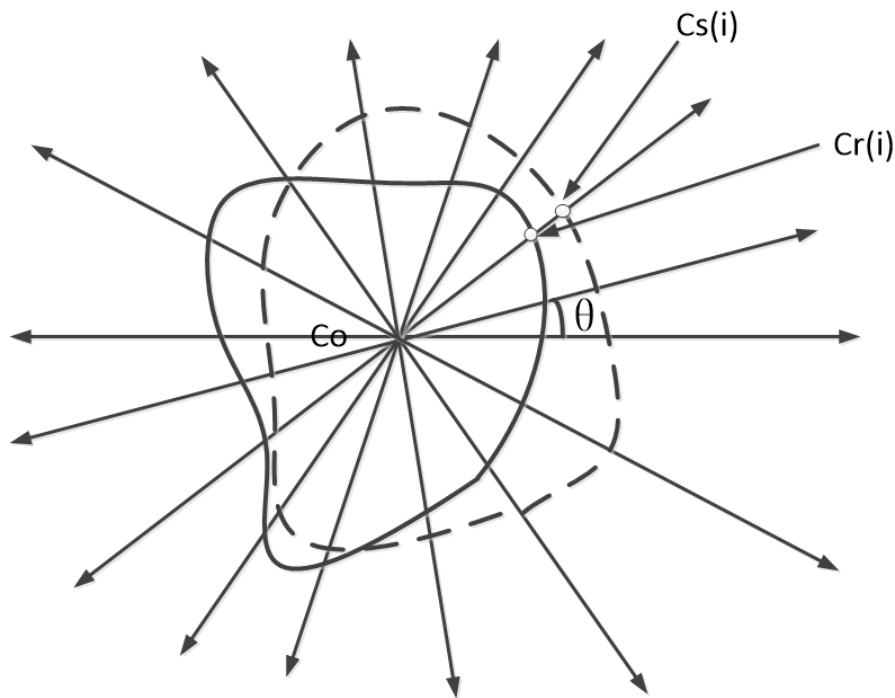


Figure 1. The computation for the averaged radical error.

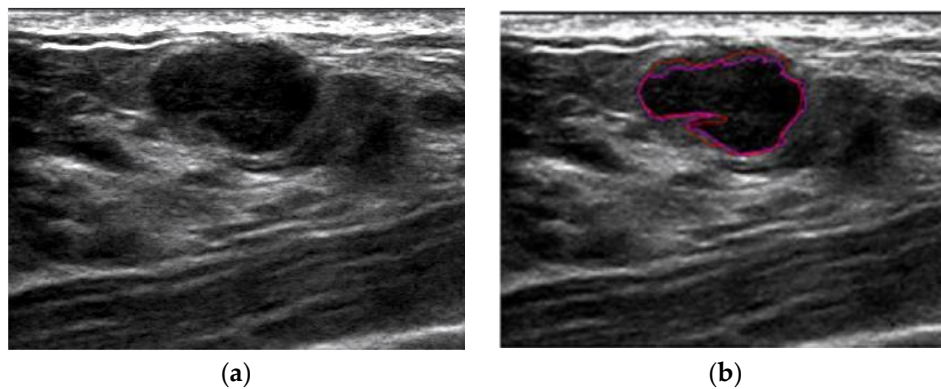


Figure 2. The segmentation result: (a) original ultrasound image; and (b) segmentation result using fuzzy C means method.

3.5. Description of Experiments

To illustrate the characteristics of the filters and their de-speckling performance, five experiments are performed. In Experiment 1, we explored the relationship between σ_d and σ_r , verified the correctness of the Equation (11), and obtained their detailed relationship curve which can result in the optimal parameters setting. The parameters for the filter are very important. In this experiment, applying the BF to filter the BUS images and tuning the value of σ_d , we aim to confirm the relationship between σ_d and σ_r similar to Equation (11) and obtain optimal σ_d and σ_r for further improvement of the BF.

In Experiment 2, by using the experiment of comparing each of PDE methods based on visual, we distinguished the performances from different PDE methods and verified that the diffusion information would affect the de-speckling effect. With drawing the relationship between φ and the VMR in PM diffusion, Equation (33) can be validated. Meanwhile, appropriate φ with appropriate number of iterative runs n could be obtained for the PDE methods. In this experiment, the PMD and

WJD are compared with each other to find the different performance between isotropic and anisotropic diffusion algorithms based on visual measurement. As typical anisotropic diffusion, the WJD can be regarded as the modified model of PMD which is typical isotropic.

In Experiment 3, we conducted the following experiments. First, we selected the edges and homogeneous regions of a specific image, and then adjust the parameters of the filters, respectively, according to the visual measurement (i.e., VMR and LRD). After that, under the radiologists' guidance, we set the parameters for each filter empirically by a number of repeated experiments. We then applied filters to the BUS images, and compute the VMR and LRD value in the homogeneous and edge region of filtered images, respectively. Additionally, comparison was taken according to VMR and LRD to analyze the performance of filters. It should be highlighted that the LRD is extremely sensitive to noise, and the LRD value makes no sense if the image is not de-noised first. To compare two filtered images, the LRD can be carried out in the case of the same VMR of two images.

In Experiment 4, the FCM algorithm [51] was utilized for BUS segmentation on the filtered images which have been filtered in Experiment 3. The ARE value can be computed so as to compare image segmentation accuracy. In this experiment, the "true" tumor regions of the ultrasound images are manually defined as the average value calculated by three radiologists. The segmentation accuracy evaluation based on the ARE for all filters investigated in this paper was calculated, and their performance were compared.

In Experiment 5, we calculated the running time of the filtering algorithms for comparison of the complexity of filtering algorithms. In this experiment, we counted completion time of eight filtering algorithms and compared their complexities.

In Experiments 3, 4, and 5, all the eight de-speckling filters adopted in this study were investigated, including WTF, GLF, WF, LF, BF, PMD, WJD, and TV. They were applied to a total of 40 ultrasound images with breast tumors (20 are benign and the rest are malignant). In all five experiments, the BUS images were provided by the Cancer Center of Sun Yat-sen University (Guangzhou, China), and taken from a SonoCT (PhilipsHDI 5000 SonoCT, ATL Philips, Eindhoven, The Netherlands) with a L12-5 50 mm Broadband Linear Array at the imaging frequency of 7.1 MHz. Each image is of 400×300 pixels in size. The simulation was carried out by Matlab 7.0 (7.0.0.19920(R14), MathWorks, Natick, MA, USA, 2004) running on a computer (MacBook Pro, Apple, San Francisco, CA, USA) with a 2.5 GHz dual-core Intel Corei5 and 4 GB of RAM. This work was approved by Human Subject Ethics Committee of South China University of Technology (Guangzhou, China).

4. Experimental Results

In this section, five groups of experimental results are presented. The first group is gained by measuring the VMR and LRD, and determining the relationship between σ_d and σ_r . The second one is obtained by comparing and analyzing image filtered by the PMD and WJD, while also testifying the relationship between VMR and diffusion function. The third group is acquired by comparing the performance of filters with appropriate parameters based on visual measurement in terms of the VMR and LRD. The fourth group is obtained by comparing the ARE of the tumor regions after image segmentation. The fifth is achieved by comparing the completion time of every filter.

4.1. Experiment 1

From the observation of Figure 3 and Table 1, we can draw a conclusion that the relationship between σ_d and σ_r nearly obeys Equation (11) where the LRD is a constant. On the whole, σ_r falls down with the increasing of the value of σ_d , see Figure 3a. Along with the increasing of the value of σ_d , the value of MR first falls sharply and at last tends to be stable, see Figure 3b.

It is concluded that the parameters of σ_d and σ_r should be set simultaneously when using the BF for the application of BUS image in order to preserve the smoothness of homogeneous region and sharpness of the edge region, simultaneously. From Figure 3, we can see that $\sigma_d = 12$ should be the best choice for the BF. In this experiment, we set σ_d in the BF to be 4, 8, 12, 16, 20, 22, and 24,

respectively, and $LRD = 0.836 \pm 0.001$ is a constant. Corresponding value of MR (1/VMR) and σ_r are shown in Table 1.

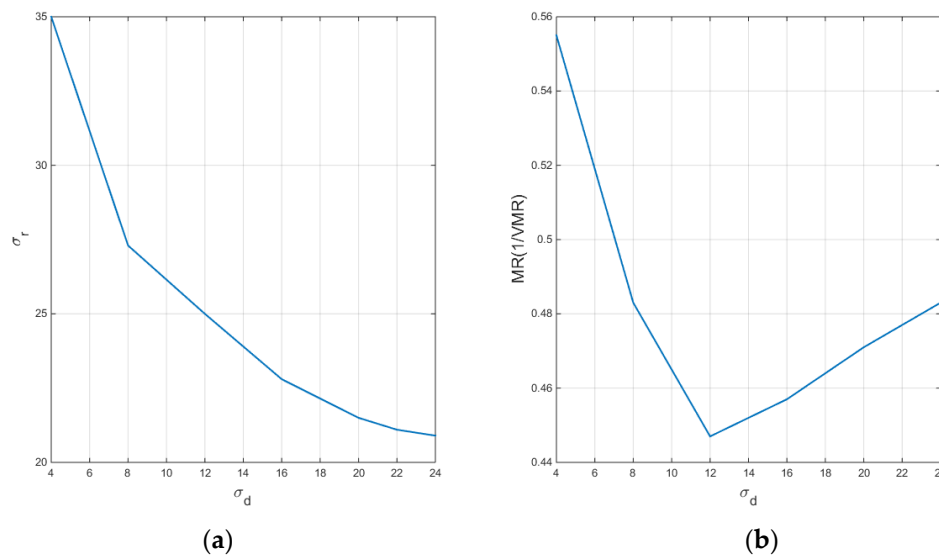


Figure 3. The relationship of σ_d , σ_r and MR (1/VMR) (MR, an intermediate variable; Mean to Variance Ratio, VMR): (a) the relationship between σ_d and σ_r ; and (b) the relationship between σ_d and MR (1/VMR).

Table 1. The MR (1/VMR) (MR, an intermediate variable; Mean to Variance Ratio, VMR) value and σ_r value that corresponding to the σ_d in the Bilateral Filter (BF).

σ_d	σ_r	MR (1/VMR)
4	35.0 ± 1.7	0.555 ± 0.038
8	27.3 ± 1.3	0.483 ± 0.027
12	25.0 ± 1.5	0.447 ± 0.025
16	22.8 ± 1.3	0.457 ± 0.017
20	21.5 ± 1.4	0.471 ± 0.016
22	21.1 ± 1.6	0.477 ± 0.021
24	20.9 ± 1.0	0.483 ± 0.022

4.2. Experiment 2

For a certain VMR value of an image before filtering, the corresponding standard deviation σ_d of the image after filtering by PMD and WJD is shown in Table 2. The σ_d of images after filtering by the PMD are much higher than those of filtering by WJD. We can come to the conclusion that WJD is less sensitive to noise than PMD model. That is to say, anisotropic diffusion shows better performance than isotropic diffusion in terms of edge preservation and de-noising.

Table 2. The σ_d value of Perona–Malik diffusion (PMD) and Weickert J Diffusion (WJD), which corresponds to MR (1/VMR).

MR (1/VMR)	0.567 ± 0.001	0.563 ± 0.001	0.552 ± 0.001	0.537 ± 0.001	0.515 ± 0.001
σ_d of PMD	1.12 ± 0.03	1.14 ± 0.02	1.18 ± 0.01	1.26 ± 0.02	1.39 ± 0.02
σ_d of WJD	0.25 ± 0.038	0.32 ± 0.038	0.38 ± 0.038	0.42 ± 0.038	0.47 ± 0.038

In this experiment, $\lambda(I_g(t)) = d(\exp(-t/K^2/2))/dt$, K is set to be 2, 4, 6, 8, and 10, respectively, and the iterative time is set to be 15. Table 3 indicates that when iterative time is kept unchanged for

15, the value of MR rises as K decreases. Therefore, we can conclude that the high φ_i leads to high degree of noise.

Table 3. The MR (1/VMR) value of PMD for different values of K , which corresponds to φ_i .

K	10	8	6	4	2
MR (1/VMR)	0.548 ± 0.011	0.585 ± 0.015	0.629 ± 0.020	0.670 ± 0.022	0.699 ± 0.025

From the observation of Figure 4e,f,h,i, the WJD model results in more continuous edge than the PMD.

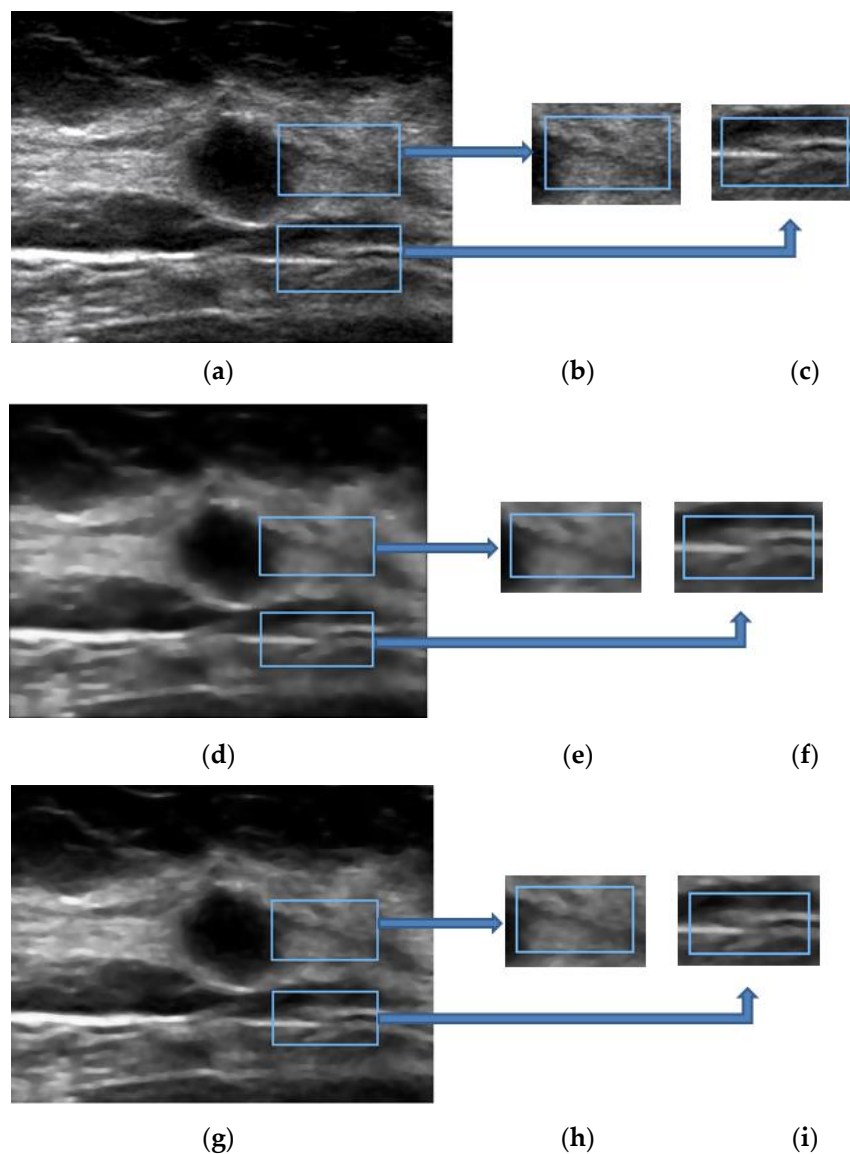


Figure 4. Visual effect between images filtered by Perona–Malik diffusion (PMD) model diffusion and Weickert J Diffusion (WJD) model diffusion: (a) original image; (b) one segment of (a); (c) another segment of (a); (d) filtered image by PMD; (e) one segment of (d); (f) another segment of (d); (g) filtered image by WJD; (h) one segment of (g); and (i) another segment of (g).

4.3. Experiment 3

In this experiment, the parameters of all filters are set under the radiologists' guidance (Table 4). σ in WF denotes as the standard deviation for degraded function, K_{SNR} is the noise to signal ratio in WF. $N_windowsize$ stands for the filter window in BF.

Table 4. The significant parameters set in the 8 filter algorithms separately.

Algorithm	Parameters
WTF	Decomposition scale is 10
GLF	$\sigma = 2$
WF	$\sigma = 4, K_{SNR} = 0.2$
LF	$\bar{n}_a = 0, \sigma_1 = 0.3, \bar{n}_m = 0, \sigma_2 = 0.02$
BF	$\sigma_d = 12, \sigma_r = 23, N_windowsize = 25$
PMD	$\sigma = 1.6, K = 10, \text{iteration No.} = 30$
WJD	$\sigma = 1.0, \Delta t = 0.25, \text{iteration No.} = 15$
TV	$\sigma = 0.08, \Delta t = 0.25, \text{iteration No.} = 15$

¹ WTF, Wavelet Transform Filter; GLF, Gaussian-Laplace Filter; WF, Wiener Filter; LF, Lee Filter; TV, Total Variation.

As shown in Table 5, it can be seen clearly that the WTF, GLF, and WF can achieve high LRD and low VMR (1/MR). Among these three filter algorithms, the WF and WTF can achieve greater clarity of edge in edge region than the GLF. For a high VMR, the LF, BF, PMD, WJD, and TV can achieve high LRD values, and their order from high to low is BF, LF, PMD, WJD, and TV. That is to say, the BF can perform best in terms of keeping clarity of edge. The performance of LF is secondary, PMD, WJD, and TV follows LF. Two groups of filtered image, including the first benign tumor image and the second malignant tumor image are shown as the example of filtering results in Figures 5 and 6.

Table 5. The visual measurement, MR (1/VMR), and Laplace Response of Domain (LRD) value of the filtered images.

Algorithm	MR (1/VMR)	LRD
WTF	0.689 ± 0.021	0.888 ± 0.017
GLF	0.642 ± 0.024	0.858 ± 0.015
WF	0.646 ± 0.030	0.903 ± 0.031
LF	0.475 ± 0.027	0.861 ± 0.025
BF	0.484 ± 0.017	0.864 ± 0.017
PMD	0.482 ± 0.016	0.844 ± 0.026
WJD	0.486 ± 0.012	0.831 ± 0.015
TV	0.488 ± 0.013	0.825 ± 0.015

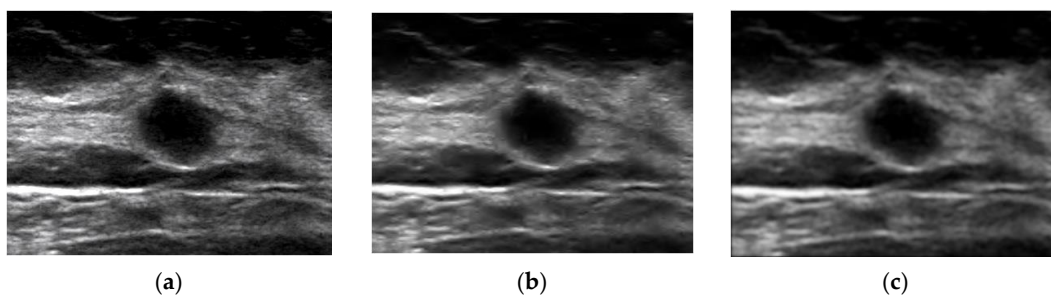


Figure 5. Cont.

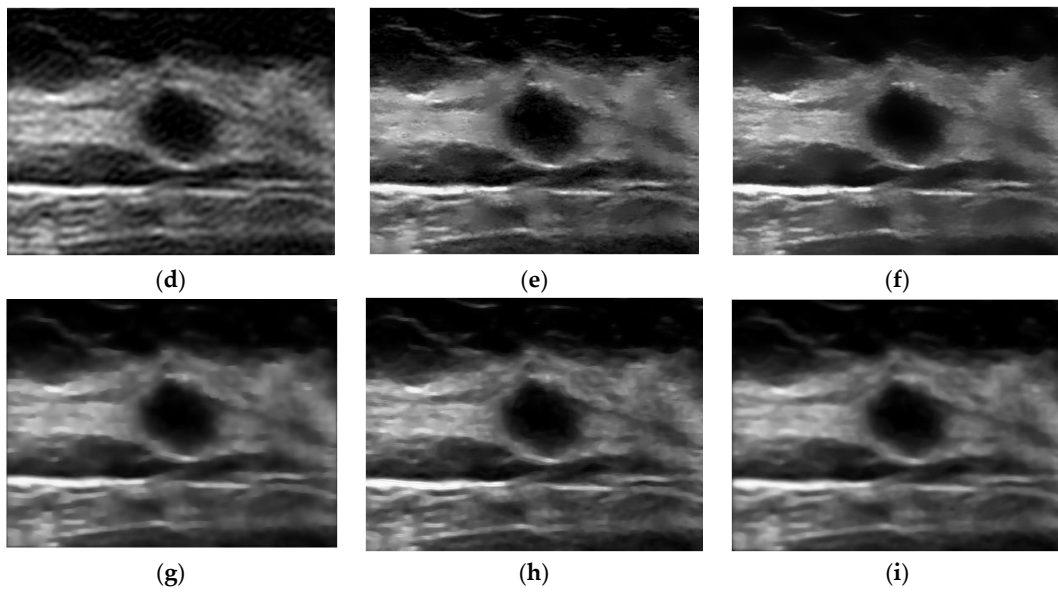


Figure 5. Image filtering results of the first benign tumor image: (a) source image; (b) Wavelet Transform Filter (WTF) result; (c) Gaussian–Laplace Filter (GLF) result; (d) Wiener Filter (WF) result; (e) Lee Filter (LF) result; (f) Bilateral Filter (BF) result; (g) PMD result; (h) WJD result; and (i) Total Variation (TV) result.

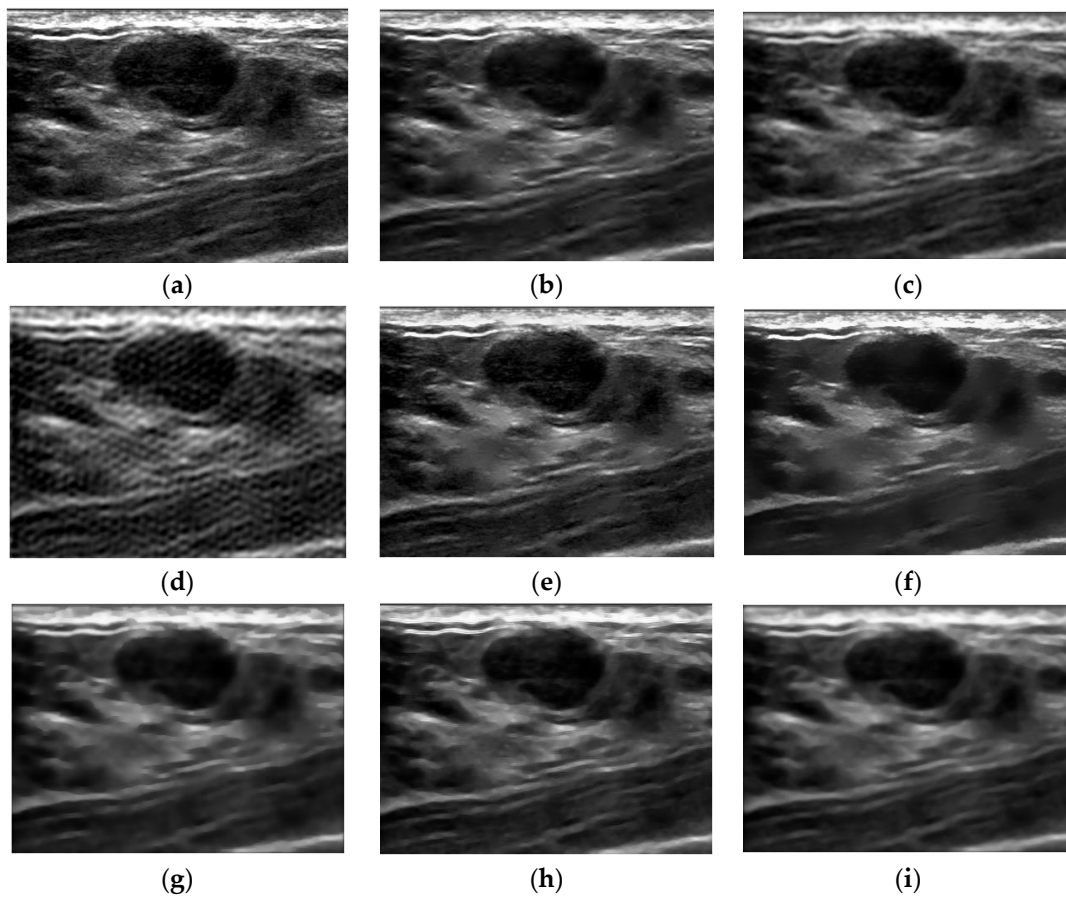


Figure 6. Image filtering results of the second malignant tumor image: (a) source image; (b) WTF result; (c) GLF result; (d) WF result; (e) LF result; (f) BF result; (g) PMD result; (h) WJD result; and (i) TV result.

4.4. Experiment 4

The ARE values of the BUS images which have been filtered in Experiment 3 were calculated in this experiment as shown in Table 6. From the results of Table 6, it is obvious that the BF with LF outperforms other filters in the metrics of ARE. However, for the images with different degrees of speckle, the ARE value indicates that the LF fluctuates more significantly compared to the BF. The WTF follows BF and LF, but its MR (1/VMR) value is very high (see Table 5). Therefore, the WTF cannot be directly suitable to the filtering process of BUS images. The WJD and TV also did a good job. In spite of good VMR, their poor LRD values lead to poor performance in tumor segmentation accuracy. Although the PMD can make the filtered image obtain higher edge retention (see Table 5), the ARE of PMD is the second worst among those filters. Taken as a whole, the PMD may not be an ideal choice for increasing tumor region segmentation accuracy. Obviously, the WF with high MR (or low VMR) values and the worst ARE is not recommended in filtering process of BUS images (see Tables 5 and 6). In other words, when the homogeneous region is seriously polluted by additive noise, it is likely that the segmentation can be corrupted, thus we tend to use filtered images with high VMR (1/MR) value.

Table 6. The results of averaged radical error (ARE) value for the filters.

Algorithm	ARE (%)
WTF	9.20 ± 1.80
GLF	9.69 ± 1.55
WF	9.87 ± 1.88
LF	9.13 ± 1.91
BF	9.10 ± 1.51
PMD	9.74 ± 1.92
WJD	9.60 ± 1.75
TV	9.56 ± 1.87

4.5. Experiment 5

From the result of Table 7, the completion time of PMD is the shortest one, and the time of GLF, WF and WTF follow it. The time of LF similar to that of BF is the median value among the whole data. The WJD owns the longest completion time that seems close to that of TV. Each completion time reflects the complexity extent of each filtering algorithm.

Table 7. The completion time of the investigated filters.

Algorithm	Time (s)
WTF	3.89 ± 0.03
GLF	3.85 ± 0.05
WF	3.81 ± 0.04
LF	6.51 ± 0.03
BF	6.91 ± 0.02
PMD	2.86 ± 0.03
WJD	11.25 ± 0.06
TV	9.50 ± 0.08

5. Discussion

From the results, it can be seen that in relation to the visual measurement perspective, a smaller variance is required from the homogeneous area of the filtering image so as to achieve a better outcome of removing the additive noise. The WTF's de-noising capability is determined by the threshold value in the wavelet domain, i.e., when the additive noise is seen as WGN, the maximum value of wavelet coefficient of noise decreases as the decomposition scale goes up. Hence, in order to get rid of the additive noise, large wavelet coefficient can be restrained in a bigger decomposition scale.

Similarly, the GLF restrains the additive noise by controlling the high frequency area. However, the edge information of an image, namely severely mutated information, mainly concentrates upon the high decomposition scale in the wavelet domain and lies in the high frequency area of the frequency domain. In the application of WTF, the decomposition scale which contains most energy of noise is difficult to determine. For the GLF, position of noise in spectrum is also hard to determine. Therefore, in relation to the preservation and reinforcement of edge, effective method is the missing link in specifically determining whether to restrain or resolve the scale and high frequency position.

The WF is widely used as an MMSE filter. However, the WF's drawbacks are obvious, i.e., its capability of suppressing the additive noise is determined by the estimation of $S_f(u, v)/S_g(u, v)$ and $H(u, v)$. Equation (13) is determined by channel estimation, but both of the former estimations cannot be accurately obtained on account of the features of medical ultrasound images. Therefore, under the circumstance where theoretical instruction is lacking, preferable capability cannot be achieved even through repeated experiments. Generally, the MMSE filter is a linear filter such that it blurs the image when reducing speckle noises [20]. Furthermore, it has been known that linear filters do not perform well in de-speckling since it blurs sharp edges [21,56].

As for the LF, its capability of de-noising for additive noise is determined by the variance of the additive noise. In addition, its ability of reversing degradation mainly depends on the variance of the multiplicative noise. Nevertheless, with regard to the medical ultrasound image, the following problems appear: (1) probability distribution function of n_m cannot be accurately estimated; (2) during the approximated evaluation of probability density function, SNR of different imaging regions are uncertain, variance of n_m cannot be accurately derived, and σ_2 remains unknown; and (3) the inevitable error existing in the estimation of variance of n_a brings major negative impact. In order to make the problems simplified, in the experiment, we gained a better ability in reversing degradation by assuming that the PDF of multiplicative noise follows Gaussian distribution $N(1, 0.02)$. On the other hand, we can easily figure it out that, theoretically, suppression of additive noise can be reached in the area where variance of n_a can be accurately estimated or the degree of degradation is weak.

As a simple algorithm, the BF is the Gaussian low pass filter which is able to make VMR ascend by reducing the noise frequency component. It proves its strong ability in eliminating additive noise in the homogeneous area. Moreover, the BF obtains favorable capability in experiments by maintaining edge information. In Equation (6), the weight of a pixel whose Euclidean distance from the central pixel being filtered is larger than σ_d can be decreased. On the other hand, the weight of a pixel will decline if its intensity difference with the central pixel which is filtered is greater than σ_r . As is indicated, it is not difficult to prove that the BF can meet the requirements of visual measurement. Moreover, depending on the results of Experiment 3 in Section 4, two conclusions can be easily drawn: (1) In order to keep the LRD from changing when increasing σ_d , σ_r must be increased simultaneously, and the relationship between σ_d and σ_r nearly obeys $\sigma_d^2 \propto 1/\sigma_r^2$ in Equation (11); and (2) VMR(1/MR) ascends as the value of σ_d goes up, yet for the purpose of keeping LRD from changing, the value of σ_d cannot be too high. Generally speaking, when the average value of σ_d and σ_r reaches more or less than 20, the BF achieves optimal outcome.

For these three filtering algorithms based on PDF, the PMD model is considered as an isotropic diffusion model for it does not consider the direction of gradient of image during the diffusion processing. The WJD and TV can be regarded as anisotropic diffusion models for they consider the diffusion direction during diffusion processing. Among these models, the PMD is the simplest one. However, compared with WJD and TV, the PMD model is more sensitive to noise and can obtain less continuous edge for the reason that it takes diffused strength into account instead of the direction. Therefore, although the PMD can get higher LRD in the case of high VMR, it does not achieve a good effect in image segmentation. With respect to the results of Experiment 2, we can promote to two conclusions:

- (1) More continuous edge obtained in anisotropic diffusion: If some part of the original edge is blurred, the diffusion at discontinuous points becomes stagnant in isotropic diffusion. However,

in anisotropic diffusion, the diffusion vertical to edge direction becomes weaker while parallel to edge direction keeps going on, which results in a more continuous edge.

- (2) Isotropic diffusion is more sensitive to noise: In isotropic diffusion, the diffusion function φ is only relevant to $|\nabla I_g(t)|$ (i.e., $|\varphi| \propto 1/|\nabla I_g(t)|$). However, in anisotropic diffusion, one diffusion function is vertical to edge (i.e., $|\varphi_{vertical}| \propto 1/|\nabla I_g(t)|$), and another diffusion function is parallel to edge (i.e., $|\varphi_{parallel}| \propto |\nabla I_g(t)|$). Therefore, in isotropic diffusion, noise exists in the homogeneous region causes discontinuous diffusion; but in anisotropic diffusion, the noise is likely to become weakened because the diffusion is vertical to edge direction.

At the same time, in Table 3, the result following Equation (34) is that the greater φ enhances the negative impact of noise. That is to say, we should set φ appropriately to reach the balance between iterative time and noise-sensitiveness. Most of the abbreviations used in this paper are described in Table A1.

6. Conclusions

In this paper, we systematically investigated eight de-speckling algorithms, the WTF, GLF, WF, LF, BF, PMD, WJD, and TV, for BUS image processing. Among the filtering algorithms in different categories, the VMR and LRD are chosen to evaluate key performance, i.e., the degree of smoothness in the homogeneous region and the clarity of detailed features in the edge region. We then demonstrate the filtering effects of these filters with respect to tumor region segmentation accuracy. Finally, referring to the experimental results, a general conclusion is drawn as the following.

In summary, speckle suppression filtering is very important when processing ultrasound images of breast tumors. In this study, it is shown that the eight typical filters all have their merits. The images filtered by the BF present a good visual effect and it is more likely to obtain good segmentation results. Additionally, it is relatively fast, and its modified model is supposed to be acceptable for real-time processing. The LF can obtain good visual result, but fluctuates significantly. The PMD is not only fast but also good at edge preservation. However, it is not suitable for being applied to the tumor region segmentation. Ultrasound images with breast tumors processed by the WJD and TV can achieve splendid segmentation accuracies. However, the searching of similar pixels in the WJD and TV will bring a heavy burden to its computation. Taking speed into account, the WJD and TV would not be good choices for de-speckling BUS images.

Acknowledgments: This work is supported by National Natural Science Funds of China (No. 61271314, 61372007, 61401286, and 61571193), the International Cooperation Project of Science and Technology of Guangdong Province (No. 2014A050503020) and Guangzhou Key Lab of Body Data Science (No. 201605030011).

Author Contributions: Qinghua Huang envisioned and coordinated the invited paper preparation; Xiaoyu Guo contributed to manuscript preparation, most of the experiments, and partial writing; Xiangfei Feng contributed to manuscript writing and paper revision including some of the experiments and experimental analysis. Xiangfei Feng and Xiaoyu Guo have made equal contribution to this paper.

Conflicts of Interest: The authors declare no conflict of interest.

Appendix

Table A1. Abbreviations and their full name in the paper.

Abbreviation	Full Name
BUS	Breast Ultrasound
MMSE	Minimum mean square error
PDE	Partial Differential Equation
VMR	Mean to Variance Ratio
LRD	Laplace Response of Domain
BF	Bilateral Filter

Table A1. Cont.

Abbreviation	Full Name
WJD	Weickert J Diffusion
TV	Total Variation
SND	Scatterer number density
FFS	Fully formed speckle
NRLR	Non-randomly distributed with long-range
NRSR	Non-randomly distributed with short-range
PDF	Probability density function
GWN	Gaussian white noise
NLM	Non-local means
PMD	Perona–Malik diffusion
NIQE	Blind image quality metric
WTF	Wavelet Transform Filter
GLF	Gaussian–Laplace Filter
LF	Lee Filter
WF	Wiener Filter
DC	Direct Current
ROI	Region of interest
FCM	Fuzzy C Mean
ARE	Averaged radial error
SSI	Speckle Suppression Index
SMPI	Speckle Suppression and Mean Preservation Index
MPSSI	Mean preservation Speckle Suppression Index

References

- Desantis, C.; Siegel, R.; Bandi, P.; Jemal, A. Breast cancer statistics, 2011. *CA Cancer J. Clin.* **2013**, *61*, 409–418. [[CrossRef](#)] [[PubMed](#)]
- Insana, M.F.; Wagner, R.F.; Garra, B.S.; Brown, D.G.; Shawker, T.H. Analysis of ultrasound image texture via generalized rician statistics. *Opt. Eng.* **1986**, *25*, 743–748. [[CrossRef](#)]
- Cardoso, F.M.; Matsumoto, M.M.S.; Furuie, S.S. Edge-preserving speckle texture removal by interference-based speckle filtering followed by anisotropic diffusion. *Ultrasound Med. Biol.* **2012**, *38*, 1414–1428. [[CrossRef](#)] [[PubMed](#)]
- Michailovich, O.V.; Tannenbaum, A. Despeckling of medical ultrasound images. *IEEE Trans. Ultrason. Ferroelectr. Freq. Control* **2006**, *53*, 64–78. [[CrossRef](#)] [[PubMed](#)]
- Bamber, J.C.; Daft, C. Adaptive filtering for reduction of speckle in ultrasonic pulse-echo images. *Ultrasonics* **1986**, *24*, 41–44. [[CrossRef](#)]
- Damodaran, N.; Ramamurthy, S.; Velusamy, S.; Manickam, G.K. Speckle noise reduction in ultrasound biomedical b-scan images using discrete topological derivative. *Ultrasound Med. Biol.* **2012**, *38*, 276–286. [[CrossRef](#)] [[PubMed](#)]
- Abdelmoniem, K.Z.; Youssef, A.B.; Kadah, Y.M. Real-time speckle reduction and coherence enhancement in ultrasound imaging via nonlinear anisotropic diffusion. *IEEE Trans. Biomed. Eng.* **2002**, *49*, 997–1014. [[CrossRef](#)] [[PubMed](#)]
- Dutt, V. Statistical Analysis of Ultrasound Echo Envelope. Ph.D. Thesis, Mayo Graduate School, Rochester, MN, USA, 1995.
- Stacy, E.W. A generalization of the gamma distribution. *Ann. Math. Stat.* **1962**, *33*, 1187–1192. [[CrossRef](#)]
- Donoho, D.L. De-noising by soft-thresholding. *IEEE Trans. Inf. Theory* **1995**, *41*, 613–627. [[CrossRef](#)]
- Guo, Y.; Cheng, H.D.; Tian, J.; Zhang, Y. A novel approach to speckle reduction in ultrasound imaging. *Ultrasound Med. Biol.* **2009**, *35*, 628–640. [[CrossRef](#)] [[PubMed](#)]
- Lee, J.S. Digital image enhancement and noise filtering by use of local statistics. *IEEE Trans. Pattern Anal. Mach. Intell.* **1980**, *2*, 165–168. [[CrossRef](#)] [[PubMed](#)]
- Kuan, D.T.; Sawchuk, A.A.; Strand, T.C.; Chavel, P. Adaptive restoration of images with speckle. *IEEE Trans. Acoust. Speech Signal Process.* **1987**, *35*, 373–383. [[CrossRef](#)]

14. Buades, A.; Coll, B.; Morel, J.M. A non-local algorithm for image denoising. In Proceedings of the IEEE Computer Society Conference on Computer Vision & Pattern Recognition, San Diego, CA, USA, 20–25 June 2005; Volume 2, pp. 60–65.
15. Coup, P.; Hellier, P.; Kervrann, C.; Barillot, C. Nonlocal means-based speckle filtering for ultrasound images. *IEEE Trans. Image Process.* **2009**, *18*, 2221–2229. [[CrossRef](#)] [[PubMed](#)]
16. Coupé, P.; Manjón, J.V.; Robles, M.; Collins, D.L. Adaptive multiresolution non-local means filter for three-dimensional magnetic resonance image denoising. *IET Image Process.* **2012**, *6*, 558–568. [[CrossRef](#)]
17. Sudeep, P.V.; Palanisamy, P.; Rajan, J.; Baradaran, H.; Saba, L.; Gupta, A.; Suri, J.S. Speckle reduction in medical ultrasound images using an unbiased non-local means method. *Biomed. Signal Process. Control* **2016**, *28*, 1–8. [[CrossRef](#)]
18. Farzana, E.; Tanzid, M.; Mohsin, K.M.; Bhuiyan, M.I.H.; Hossain, S. Adaptive bilateral filtering for despeckling of medical ultrasound images. In Proceedings of the TENCON 2010—2010 IEEE Region 10 Conference, Fukuoka, Japan, 21–24 November 2010; pp. 1728–1733.
19. Aysal, T.C.; Barner, K.E. Rayleigh-maximum-likelihood filtering for speckle reduction of ultrasound images. *IEEE Trans. Med. Imaging* **2007**, *26*, 712–727. [[CrossRef](#)] [[PubMed](#)]
20. Eom, K.B. Speckle reduction in ultrasound images using nonisotropic adaptive filtering. *Ultrasound Med. Biol.* **2011**, *37*, 1677–1688. [[CrossRef](#)] [[PubMed](#)]
21. Touzi, R. A review of speckle filtering in the context of estimation theory. *IEEE Trans. Geosci. Remote Sens.* **2002**, *40*, 2392–2404. [[CrossRef](#)]
22. Jin, J.S.; Wang, Y.; Hiller, J. An adaptive nonlinear diffusion algorithm for filtering medical images. *IEEE Trans. Inf. Technol. Biomed.* **2000**, *4*, 298–305. [[CrossRef](#)] [[PubMed](#)]
23. Perona, P.; Malik, J. Scale-space and edge detection using anisotropic diffusion. *IEEE Trans. Pattern Anal. Mach. Intell.* **1990**, *12*, 629–639. [[CrossRef](#)]
24. Weickert, J. *A Review of Nonlinear Diffusion Filtering*; Springer: Berlin/Heidelberg, Germany, 1997; pp. 1–28.
25. Rudin, L.I.; Osher, S.; Fatemi, E. Nonlinear total variation based noise removal algorithms. *Phys. D Nonlinear Phenom.* **1992**, *60*, 259–268. [[CrossRef](#)]
26. Loizou, C.P.; Pattichis, C.S.; Christodoulou, C.I.; Istepanian, R.S.H.; Pantziaris, M.; Nicolaidis, A. Comparative evaluation of despeckle filtering in ultrasound imaging of the carotid artery. *IEEE Trans. Ultrason. Ferroelectr. Freq. Control* **2005**, *52*, 1653–1669. [[CrossRef](#)] [[PubMed](#)]
27. Finn, S.; Glavin, M.; Jones, E. Echocardiographic speckle reduction comparison. *IEEE Trans. Ultrason. Ferroelectr. Freq. Control* **2011**, *58*, 82–101. [[CrossRef](#)] [[PubMed](#)]
28. Manth, N.; Virmani, J.; Kumar, V.; Kalra, N. Despeckle filtering: Performance evaluation for malignant focal hepatic lesions. In Proceedings of the 2015 2nd International Conference on Computing for Sustainable Global Development, New Delhi, India, 11–13 March 2015; pp. 1897–1902.
29. Zhang, J.; Wang, C.; Cheng, Y. Comparison of despeckle filters for breast ultrasound images. *Circuits Syst. Signal Process.* **2015**, *34*, 185–208. [[CrossRef](#)]
30. Kaur, A.; Kaur, S. Comparative analysis of various spatial filters for de-speckling ultrasound images. *Imp. J. Interdiscip. Res.* **2016**, *2*, 1459–1467.
31. Anfinson, S.N.; Doulgeris, A.P.; Eltoft, T. Estimation of the equivalent number of looks in polarimetric SAR imagery. In Proceedings of the 2008 IEEE International Geoscience and Remote Sensing Symposium (IGARSS), Boston, MA, USA, 7–11 July 2008; pp. IV-487–IV-490.
32. Gonzalez, R.C.; Woods, R.E. *Digital Image Processing*, 2nd ed.; Addison-Wesley Longman Publishing Co.: Boston, MA, USA, 1992.
33. Bhuiyan, M.I.H.; Ahmad, M.O.; Swamy, M.N.S. Spatially adaptive thresholding in wavelet domain for despeckling of ultrasound images. *IET Image Process.* **2009**, *3*, 147–162. [[CrossRef](#)]
34. Mustafa, N.; Li, J.P.; Khan, S.A.; Giess, M. Medical image de-noising schemes using wavelet threshold techniques with various noises. In Proceedings of the 2015 12th International Computer Conference on Wavelet Active Media Technology and Information Processing (ICCWAMTIP), Chengdu, China, 18–20 December 2015; pp. 283–289.
35. Yadav, A.K.; Roy, R.; Kumar, A.P.; Kumar, C.S.; Dhakad, S.K. De-noising of ultrasound image using discrete wavelet transform by symlet wavelet and filters. In Proceedings of the 2015 International Conference on Advances in Computing, Communications and Informatics (ICACCI), Kochi, India, 10–13 August 2015; pp. 1204–1208.

36. Wang, D.; Zhang, C.; Zhao, X. Multivariate laplace filter: A heavy-tailed model for target tracking. In Proceedings of the 19th International Conference on Pattern Recognition, Tampa, FL, USA, 8–11 December 2008; pp. 1–4.
37. Chen, S.; Yao, L.; Chen, B. A parameterized logarithmic image processing method with laplacian of gaussian filtering for lung nodule enhancement in chest radiographs. *Med. Biol. Eng. Comput.* **2016**, *54*, 1793–1806. [[CrossRef](#)] [[PubMed](#)]
38. Lee, J.S. Speckle analysis and smoothing of synthetic aperture radar images. *Comput. Graph. Image Process.* **1981**, *17*, 24–32. [[CrossRef](#)]
39. Zhong, H.; Lu, L.; Jiao, L. Fast non-local lee filter for SAR image despeckling using directional projection. In Proceedings of the 2011 IEEE CIE International Conference on Radar, Chengdu, China, 24–27 October 2011; Volume 2, pp. 1600–1603.
40. Hazarika, D.; Nath, V.K.; Bhuyan, M. In A lapped transform domain enhanced lee filter with edge detection for speckle noise reduction in sar images. In Proceedings of the 2015 IEEE 2nd International Conference on Recent Trends in Information Systems (ReTIS), Kolkata, India, 9–11 July 2015; pp. 243–248.
41. Insana, M.F.; Hall, T.J.; Cox, G.G.; Rosenthal, S.J. Progress in quantitative ultrasonic imaging. *Proc. SPIE Int. Soc. Opt. Eng.* **1989**, *1090*, 2–9.
42. Aurich V, W.J. Non-linear gaussian filters performing edge preserving diffusion. In *Mustererkennung*; Springer: Berlin/Heidelberg, Germany, 1995; pp. 538–545.
43. Tomasi, C.; Manduchi, R. Bilateral filtering for gray and color images. In Proceedings of the Sixth International Conference on Computer Vision, Bombay, India, 7 January 1998; pp. 836–846.
44. Wiener, N. *Extrapolation and Smoothing of Stationary Time Series*; MIT Press: Cambridge, MA, USA, 1949.
45. Juang, P.A.; Wu, M.N. Ultrasound speckle image process using wiener pseudo-inverse filtering. In Proceedings of the 33rd Annual Conference of the IEEE Industrial Electronics Society (IECON 2007), Taipei, Taiwan, 5–8 November 2007; pp. 2446–2449.
46. Rao, A.R.; Schunck, B.G. Computing oriented texture fields. In Proceedings of the IEEE Computer Society Conference on Computer Vision & Pattern Recognition, San Diego, CA, USA, 4–8 June 1989; pp. 157–185.
47. Wang, L.; Xiao, L.; Huang, L.; Wei, Z. Nonlocal total variation based speckle noise removal method for ultrasound image. *Int. Congr. Image Signal Process.* **2011**, *2*, 709–713.
48. Sheng, Y.; Xia, Z.G. A comprehensive evaluation of filters for radar speckle suppression. In Proceedings of the ‘Remote Sensing for a Sustainable Future’, International Geoscience and Remote Sensing Symposium (IGARSS ’96), Lincoln, NE, USA, 27–31 May 1996; Volume 1553, pp. 1559–1561.
49. Shamsoddinia, A.; Trinder, J.C. Image texture preservation in speckle noise suppression. In Proceedings of the ISPRS TC VII Symposium, Vienna, Austria, 5–7 July 2010.
50. Dellepiane, S.G.; Angiati, E. Quality assessment of despeckled SAR images. *IEEE J. Sel. Top. Appl. Earth Obs. Remote Sens.* **2014**, *7*, 691–707. [[CrossRef](#)]
51. Moon, W.K.; Lo, C.M.; Chen, R.T.; Shen, Y.W.; Chang, J.M.; Huang, C.S.; Chen, J.H.; Hsu, W.W.; Chang, R.F. Tumor detection in automated breast ultrasound images using quantitative tissue clustering. *Med. Phys.* **2014**, *41*, 042901. [[CrossRef](#)] [[PubMed](#)]
52. Huang, Q.H.; Lee, S.Y.; Liu, L.Z.; Lu, M.H.; Jin, L.W.; Li, A.H. A robust graph-based segmentation method for breast tumors in ultrasound images. *Ultrasonics* **2012**, *52*, 266–275. [[CrossRef](#)] [[PubMed](#)]
53. Chang, H.L.; Chen, Z.P.; Huang, Q.H.; Shi, J.; Li, X.L. Graph-based learning for segmentation of 3D ultrasound images. *Neurocomputing* **2015**, *151*, 632–644. [[CrossRef](#)]
54. Huang, Q.H.; Yang, F.B.; Liu, L.Z.; Li, X.L. Automatic segmentation of breast lesions for interaction in ultrasonic computer-aided diagnosis. *Inf. Sci.* **2015**, *314*, 293–310. [[CrossRef](#)]
55. Huang, Q.H.; Bai, X.; Li, Y.G.; Jin, L.W.; Li, X.L. Optimized graph-based segmentation for breast ultrasound. *Neurocomputing* **2014**, *129*, 216–224. [[CrossRef](#)]
56. Shreyamsha Kumar, B.K. Image denoising based on non-local means filter and its method noise thresholding. *Signal Image Video Process.* **2013**, *7*, 1211–1227. [[CrossRef](#)]

